

RESEARCH

Open Access

# Experimental measurement of surface strains and local lattice rotations combined with 3D microstructure reconstruction from deformed polycrystalline ensembles at the micro-scale

Paul A Shade\*, Michael A Groeber, Jay C Schuren and Michael D Uchic

\* Correspondence:  
paul.shade.1@us.af.mil  
Air Force Research Laboratory,  
Materials and Manufacturing  
Directorate, 2230 10th Street,  
Wright-Patterson AFB, OH 45433, USA

## Abstract

This article describes a new approach to characterize the deformation response of polycrystalline metals using a combination of novel micro-scale experimental methodologies. An in-situ scanning electron microscope (SEM)-based tension testing system was used to deform micro-scale polycrystalline samples to modest and moderate plastic strains. These tests included measurement of the local displacement field with nm-scale resolution at the sample surface. After testing, focused ion beam serial sectioning experiments that incorporated electron backscatter diffraction mapping were performed to characterize both the internal 3D grain structure and local lattice rotations that developed within the deformed micro-scale test samples. This combination of experiments enables the local surface displacements and internal lattice rotations to be directly correlated with the underlying 3D polycrystalline microstructure, and such information can be used to validate and guide further development of modeling and simulation methods that predict the local plastic deformation response of polycrystalline ensembles.

**Keywords:** Micro-tensile test; Plastic deformation; Microstructure

## Background

Many structural components are fabricated from polycrystalline materials, and the desire to both optimize the performance and extend the lifetime of metallic alloys has fostered the development of advanced micromechanical modeling and simulation tools that can accurately predict the deformation response of polycrystalline ensembles. Experimental and computational techniques working toward this goal have been the subject of numerous studies, and have evolved with increasing fidelity at decreasing length scales. One example of many approaches to address this need is crystal plasticity finite element modeling (CP-FEM) focused on explicitly representing the morphology and local crystallographic orientations of polycrystalline microstructures [1]. These models can predict the development of intra- and inter-granular gradients in the deformation field, as well as the evolution of grain morphology and local lattice rotations, and yet at the same time have known limitations such as the inability to accurately account for length scale effects [2-4].

Experimental validation of such methods is critical to guide their further development and implementation. However, due to experimental and computational challenges, validation studies which compare experimental data to simulations which explicitly incorporate the experimental microstructure have been historically limited. These have largely involved studies where only the surface microstructure of a mechanical test specimen has been experimentally determined and subsequently used as input for either 2D or quasi-3D simulations [5-7], or to approximate the 3D microstructure of a simplified material (i.e., very large grain materials where the sub-surface microstructure is assumed to be columnar) [8-12]. St-Pierre collected 2D electron backscatter diffraction (EBSD) scans of the surface microstructure of a tensile sample and used microstructure statistics to generate a 3D mesh of the tensile sample with the experimental surface and a realistic sub-surface virtual microstructure [13]. Musienko utilized successive electropolishing on a post-deformation tensile specimen combined with EBSD scans to determine the 3D microstructure from a small volume in a region-of-interest near the specimen surface, which was subsequently meshed and simulated to compare to the tensile experiment [14].

In the present study, we demonstrate a new methodology for generating mechanical test datasets combined with explicit microstructure representation of the entire test specimen. We have employed in-situ SEM-based micro-scale tensile testing [15-18] combined with surface strain mapping to track the evolution of surface strains throughout the mechanical test [19-23]. Micro-scale test volumes are amenable to 3D serial sectioning in focused ion beam-scanning electron microscopes (FIB-SEM), and performing such experiments while incorporating EBSD mapping allows for capturing the post-deformation microstructure, including local lattice rotations [24-27]. The combination of all of these techniques allows the collection of rich datasets for model development and validation studies; these efforts are described in other publications [28].

## **Methods, results and discussion**

### **Sample preparation**

The material selected for this work was a 99.0% purity annealed Ni foil with a nominal thickness of 50  $\mu\text{m}$ . The foil contained no appreciable texture and was comprised of equiaxed grains with an average diameter of approximately 10  $\mu\text{m}$ . Micro-tensile samples were fabricated from the foil by implementing a stencil mask technique [29]. This technique involves using standard microelectronics processing methods to produce high aspect-ratio stencil masks from a Si wafer. Once fabricated, the stencil masks are placed on top of the foil and the mask-and-foil are co-sputtered using a broad ion beam milling system. This ultimately transfers the pattern of the stencil mask into the foil, creating an array of test structures. For the present experiments, the Si wafer was 200  $\mu\text{m}$  in thickness and the pattern consisted of an array of tensile samples integrally attached to the bulk substrate. Milling was conducted with a Gatan Precision Etching Coating System, operated with a 6 kV  $\text{Ar}^+$  broad ion beam for approximately 40 hours.

After completing the stencil mask procedure described above, the Ni tensile samples required further micro-machining to remove both tapered sidewalls and a thin coating of re-deposited material. An FEI Nova 600 Dual Beam FIB-SEM was used to perform these tasks. First, the top and bottom surfaces of the samples were milled to remove

any re-deposited material and also to thin the specimens to the desired thickness. Surface striations, a.k.a. “curtaining”, invariably developed during this process because of the relatively large dimensions of the specimens for ion milling which required the use of relatively large beam currents for the final microfinishing step ( $> 5$  nA), as can be seen in Figure 1. Following this, an automated procedure was developed and implemented to remove the taper from the specimen sidewalls. This procedure combined motorized microscope stage movements with image recognition-optimized placement of milling patterns to iteratively cross-section mill the perimeter of the sample while maintaining a biased back-tilt of  $1^\circ$  relative to the sidewall. This allowed nearly perfectly orthogonal sidewalls to be produced.

Three samples were fabricated with a final specimen geometry consisting of a rectangular cross section, a gage width of  $21\ \mu\text{m}$ , a thickness of  $38\ \mu\text{m}$ , and a gage length of  $80\ \mu\text{m}$ . Images of the samples prior to testing can be seen in Figure 1. The flat sample surfaces were conducive to collecting EBSD patterns before and after mechanical testing, and also for making surface strain measurements throughout the mechanical test. The choice of material, grain size and specimen dimensions allowed for roughly 200 grains to be included in the gage volume. This allowed the experiment to include a sufficient number of grains such that the results would be relevant to interrogating a polycrystalline response, yet have the total number of grains be small enough such that

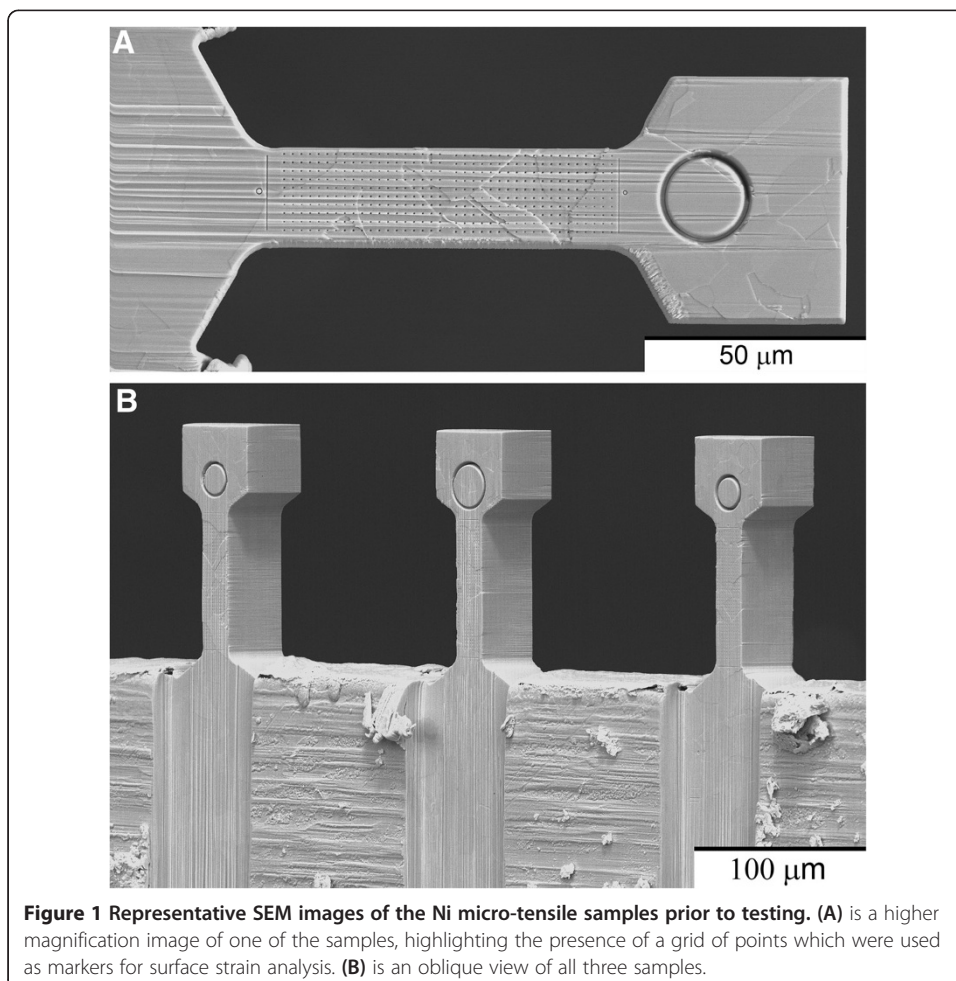


**Figure 1** Representative SEM images of the Ni micro-tensile samples prior to testing. (A) is a higher magnification image of one of the samples, highlighting the presence of a grid of points which were used as markers for surface strain analysis. (B) is an oblique view of all three samples.

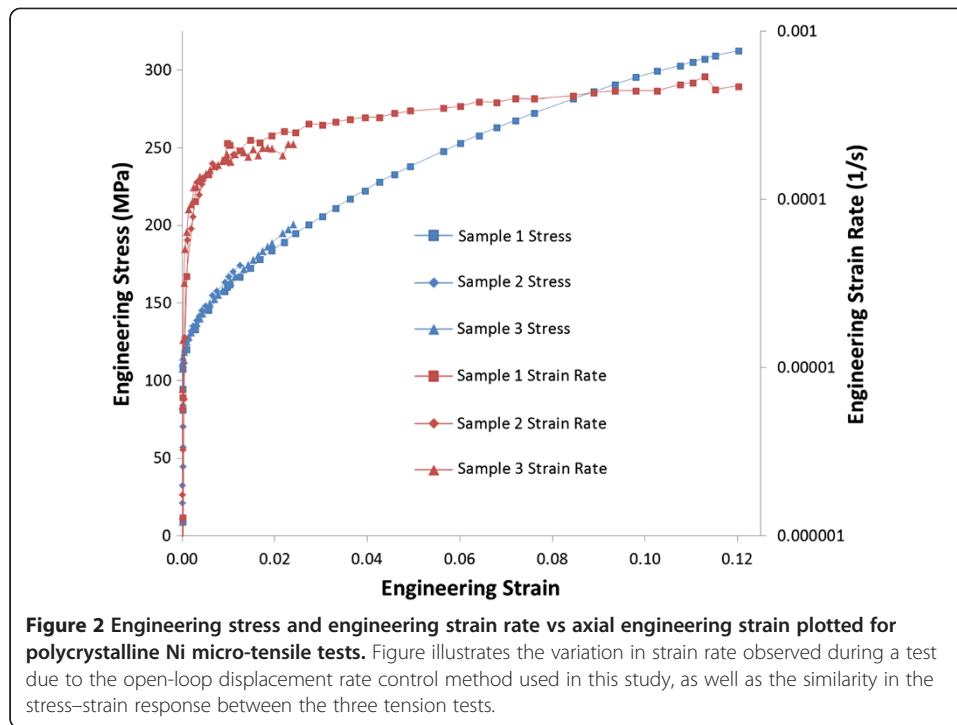
the test could still be directly simulated using a CP-FEM model instantiated with the explicit 3D microstructure [28]. Furthermore, the specimen dimensions are appropriate for micro-tensile testing and post-test 3D-EBSD serial sectioning in the FIB-SEM.

### **Mechanical testing**

In-situ SEM-based micro-tensile testing was conducted using a custom-built mechanical testing device [18,30,31]. Selected details of the device construction have been reported elsewhere [31]. The device is displacement-controlled using a piezoelectric actuator, and load is measured with a strain-gage-based load cell. The local sample displacements are calculated from SEM images by tracking the positional change of distinct features on the specimen surface. An alignment flexure ensures linear motion of the loading train [32,33], and the samples are precisely positioned for testing by attaching the bulk substrate to a piezoelectric controlled x-y-z micro-positioning stage. The FIB-SEM was used to manufacture a tensile grip into the end of a SiC fiber which was 8 mm in length and 0.1 mm in diameter, and attached at the other end to the load cell. The 80:1 aspect ratio of the SiC fiber enables the tensile grip to have an extremely low lateral stiffness, thus minimizing the lateral constraints imposed on the specimen during mechanical testing [18,31]. As a result, the imposed boundary conditions are different from that in a traditional tensile test.

The mechanical tests were conducted in-situ in an FEI Sirion SEM equipped with a 4 pi image acquisition system. The recorded images had dimensions that were  $6000 \times 2000$  pixels, corresponding to a pixel size of  $\sim 2$  nm, and contained 16 bit depth. The tests were conducted in a quasi-static manner, where the samples underwent sequential periods of loading at a constant actuator voltage ramp rate (open-loop displacement rate control) separated by periods in which the actuator was held at a constant voltage to facilitate the collection of high resolution SEM images. While the voltage ramp rate of the actuator was held constant during the loading portions of each test, i.e., the actuator displaced a constant amount for each loading segment, the displacement achieved by the sample varied due to the high compliance of the load cell. This is illustrated in Figure 2, which shows a plot of stress and strain rate vs strain for the three tested samples, where it can be seen that the strain rates were initially very low during elastic loading and increased rapidly until reaching a more stable rate once each sample started to plastically deform. Note that the strain rate values reported were calculated by measuring the change in engineering strain between two images and dividing by the period of time over which the voltage values supplied to the actuator were increased. Therefore, the strain rate values reported are actually an upper limit estimate, as they do not account for the possibility of creep in the sample while the load is held static during image collection. For strain rate sensitive materials this mode of testing may significantly affect the results, however, the impact is expected to be minimal for Ni polycrystals. Due to the relatively high elastic modulus ( $\sim 200$  GPa) and low yield stress ( $\sim 100$  MPa) of the Ni foil, total elastic strain values for the samples corresponded to displacement values of only about 2 pixels, and therefore it was not possible to accurately measure elastic modulus values from these experiments.

The three samples were tested to different strain levels ( $\sim 1.1$ , 2.5, and 11.9% axial engineering strain), as shown in Figure 2. Despite the limited number of grains within



the gage volume and expected variation in local grain configurations among the three samples, the three engineering stress-strain curves are very similar. This agreement highlights the potential limitation of using the global stress-strain response as a sole validation metric, and thus other measures are required for interrogating the plastic deformation behavior of polycrystalline ensembles.

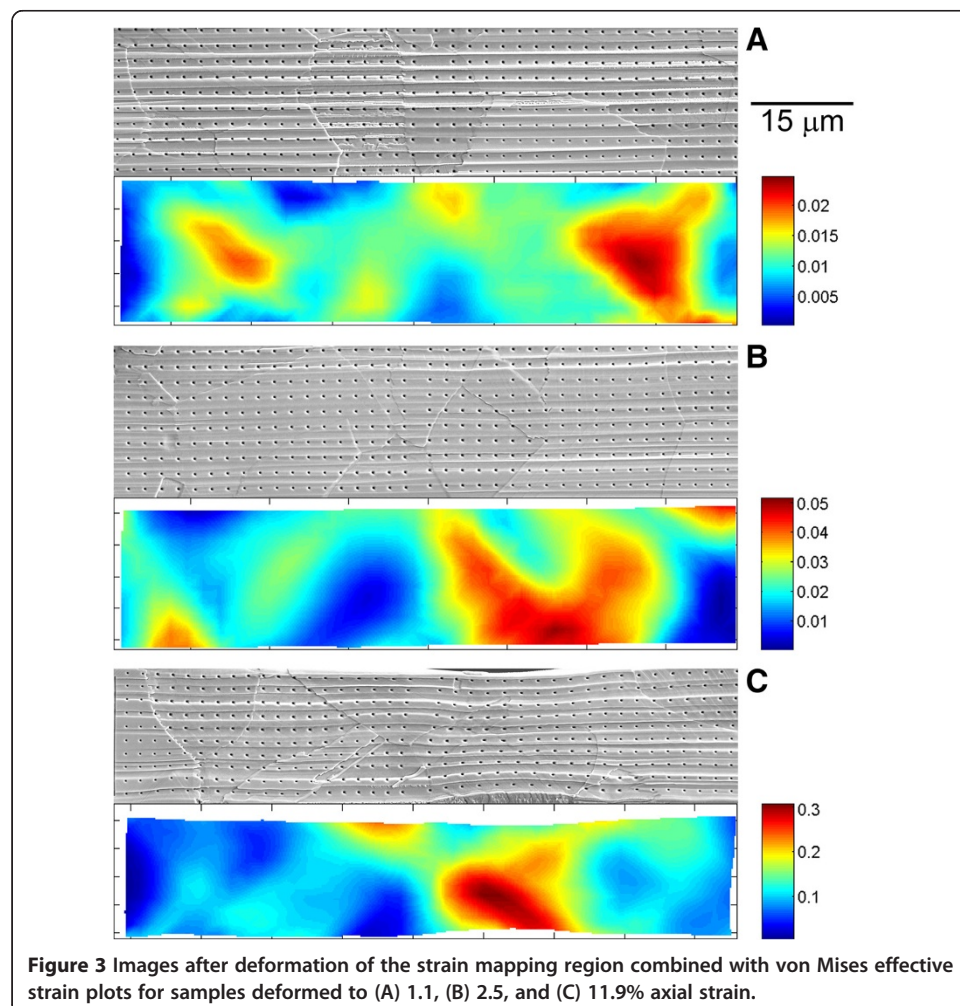
### Surface strain mapping

The evolution and distribution of surface strains is typically a direct output of modeling tools such as CP-FEM, and these quantities are also measurable using modern digital image correlation (DIC) methods [8,10,12-14]. Both random and regular patterns can be used for DIC analysis, and for the present study a regular grid of points was milled onto the top surface of the micro-tensile samples prior to testing using the FIB-SEM. The markers (points) were circular with an approximate diameter of 30 nm and a point-to-point spacing of 2.3  $\mu\text{m}$ . An example of this marker pattern can be seen in Figure 1A.

The distortion of the grid throughout an experiment was measured from the individual images and used to determine local surface strains, following a methodology similar to that described by Biery et al. [23]. First, marker positions in each image were determined using a script that quickly found rough marker coordinates by performing a binary segmentation with a threshold intensity value that highlighted the markers, and then calculated the centroid of the resulting cluster of pixels at each marker. Refined coordinates were subsequently determined with sub-pixel accuracy by calculating the peak positions of a 2D Gaussian fit around each marker in the original non-segmented images. Marker positions in the image prior to testing were taken as a reference, and

second order polynomial fits were calculated that mapped the positions of a central marker and the nearest surrounding markers in the reference image to those in the distorted image. Strain values were then determined from the coefficients of the polynomial fits following equations 1–3 from Biery et al. [23].

Figure 3 shows images of the deformed grid in the strain mapping region combined with von Mises effective strain plots, where the von Mises effective strain was calculated using equation 1 from Wu et al. [34]. Note the strongly heterogeneous nature of the strain distribution in all three samples, where some regions remain nearly undeformed while others contain strains which are on the order of double the average value. For example, the sample deformed to 1.1% axial strain had local axial strain values that ranged from  $-0.2$  to  $2.3\%$  with a standard deviation of  $0.4\%$ . The difference is magnified in the higher strain samples, where the sample deformed to  $2.5\%$  axial strain had local axial strain values that ranged from  $-0.3$  to  $5.0\%$  with a standard deviation of  $1.2\%$ , and the sample deformed to  $11.9\%$  axial strain had local axial strain values that ranged from  $-0.8$  to  $30.8\%$  with a standard deviation of  $6.1\%$ . Videos which show the evolution of the axial (XX), transverse (YY), and in-plane shear (XY) surface strain distribution, along with the surface strain mapping region and stress–strain plot,



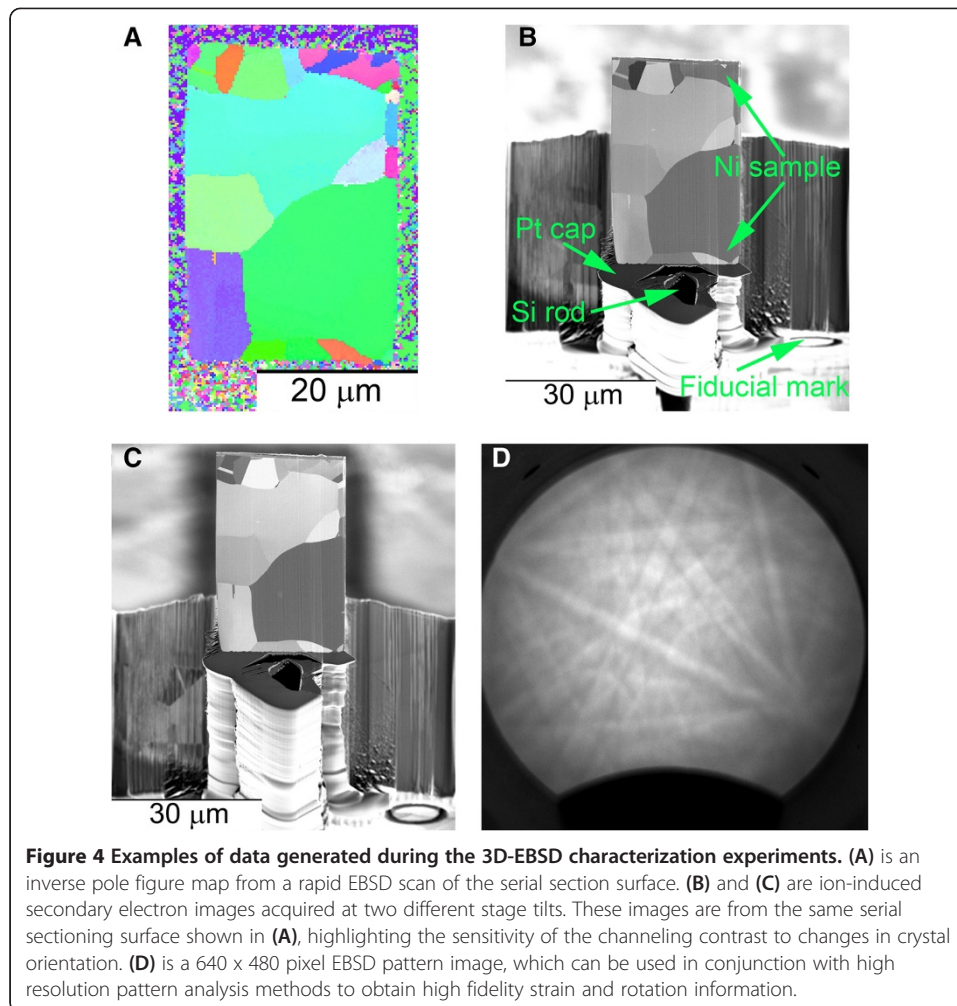
for all three samples are available in the online version of this manuscript (Additional files 1, 2 and 3).

### **3D-EBSD serial sectioning**

The internal microstructures of the deformed samples were characterized following mechanical testing by 3D-EBSD serial sectioning using the aforementioned FIB-SEM equipped with a TSL Hikari EBSD detector. The 3D-EBSD serial sectioning process has been described in detail elsewhere [24-27]. Briefly, the process consisted of repeated cross-section milling of the sample using the ion beam, followed by repositioning the sample via tilt, rotation and translation of the 5-axis microscope stage to collect a variety of images or crystallographic (EBSD) maps for each section. This process has been fully automated with the development of custom codes that utilize FEI RunScript software to control the FIB-SEM, and AutoIt automation software to initiate the collection of EBSD maps and facilitate communication between the FIB-SEM control computer and the EBSD acquisition system.

Prior to collection of the 3D-EBSD data, a  $\sim 3 \mu\text{m}$  thick layer of Pt was deposited onto the specimen surface and a series of fiducial markers for fine scale positioning were milled into the bulk substrate near the tensile sample. These fiducial markers are used in conjunction with image matching algorithms to optimize the kinematic position of the sample prior to ion milling or data acquisition, and also allow for precise placement of ion milling patterns to minimize the effects of sample drift or minor variability in sample positioning. Cross-section milling was conducted with a 30 kV  $\text{Ga}^+$  ion beam at a current of 6.5 nA. The cross-sections were milled with a  $1^\circ$  back-tilt to compensate for taper of the cross-section surface, and the incremental section thickness was approximately 250 nm. Crystallographic orientation information was captured for each section by collecting EBSD maps, using a 20 kV accelerating voltage and 250 nm pixel size. The grain structure was also imaged using ion-induced secondary electron (ISE) images using a 30 kV  $\text{Ga}^+$  ion beam and a current of 0.1 nA, resulting in an in-plane resolution of  $\sim 50$  nm. These ISE images display significant channeling contrast for polycrystalline grain structures [24,35] and were collected at two different tilt values to increase the probability of having at least one ISE image where all neighboring grain pairs displayed visibly different gray-scale intensities. However, due to the long time duration of these experiments, the intensity of the ISE images varied dramatically over the course of the serial sectioning experiment (which we attributed to slowly-varying changes in the current delivered to the sample by the ion column), and as a result a number of the ISE images had poor contrast that prevented the use of image processing methods to segment the internal grain structure. Examples of the various data collected for each section are shown in Figure 4. Each 3D-EBSD dataset consisted of approximately 400 sections and required approximately 6 days of collection time.

Additionally, for one of the samples the raw EBSD patterns were saved for every pixel within a scan. Enabling this option significantly slows the acquisition process, in part because of the requirement to not use pattern binning and additionally to allow time for the computer to store large quantities of image data. As such, the raw EBSD pattern data was collected with a reduced resolution of  $1 \mu\text{m}$  voxels by using an in-plane pixel size of  $1 \mu\text{m}$  and only collecting this data for every fourth cross-section. The resolution



of the pattern images was  $640 \times 480$ , an example of which can be seen in Figure 4D. A single crystal Si rod was extracted from a wafer and placed on top of the sample using an Omniprobe micro-manipulator to be used as a pattern center reference (as can be seen in Figure 4B and C), however, differences between Si and Ni diffraction pattern intensities made it difficult to find a set of camera parameters optimized for both and as such the pattern quality in this experiment was insufficient for this application. Currently, the raw EBSD patterns are not being used, however, in the future we hope to use this data to extract residual strains along with more precise crystallographic orientations [36].

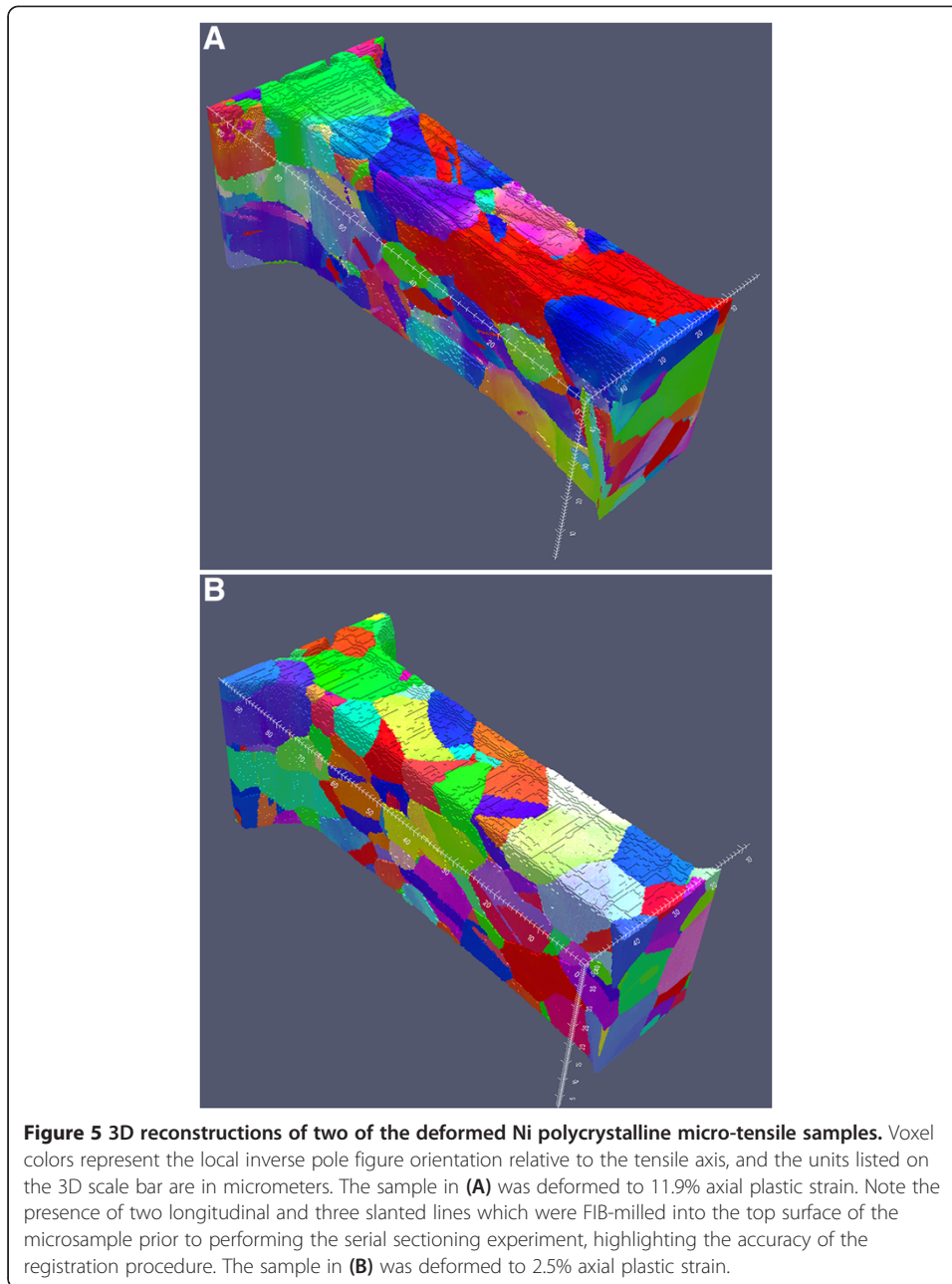
The series of individual 2D EBSD maps were aligned and reconstructed [37,38] using DREAM.3D software [39] to produce a 3D volume. The procedure used to register, segment and reconstruct the 3D EBSD data in DREAM.3D is the following. After importing the original series of EBSD scans, the sample volume was identified from the empty space surrounding the sample by using a multiple threshold criteria. For the data sets shown, we have selected threshold values for both image quality [40] and confidence index of the EBSD data that correctly identified most of the voxels associated with the sample volume, with some misclassified voxels internal to the sample as well as in the empty space surrounding the sample. Next, gross section-to-section



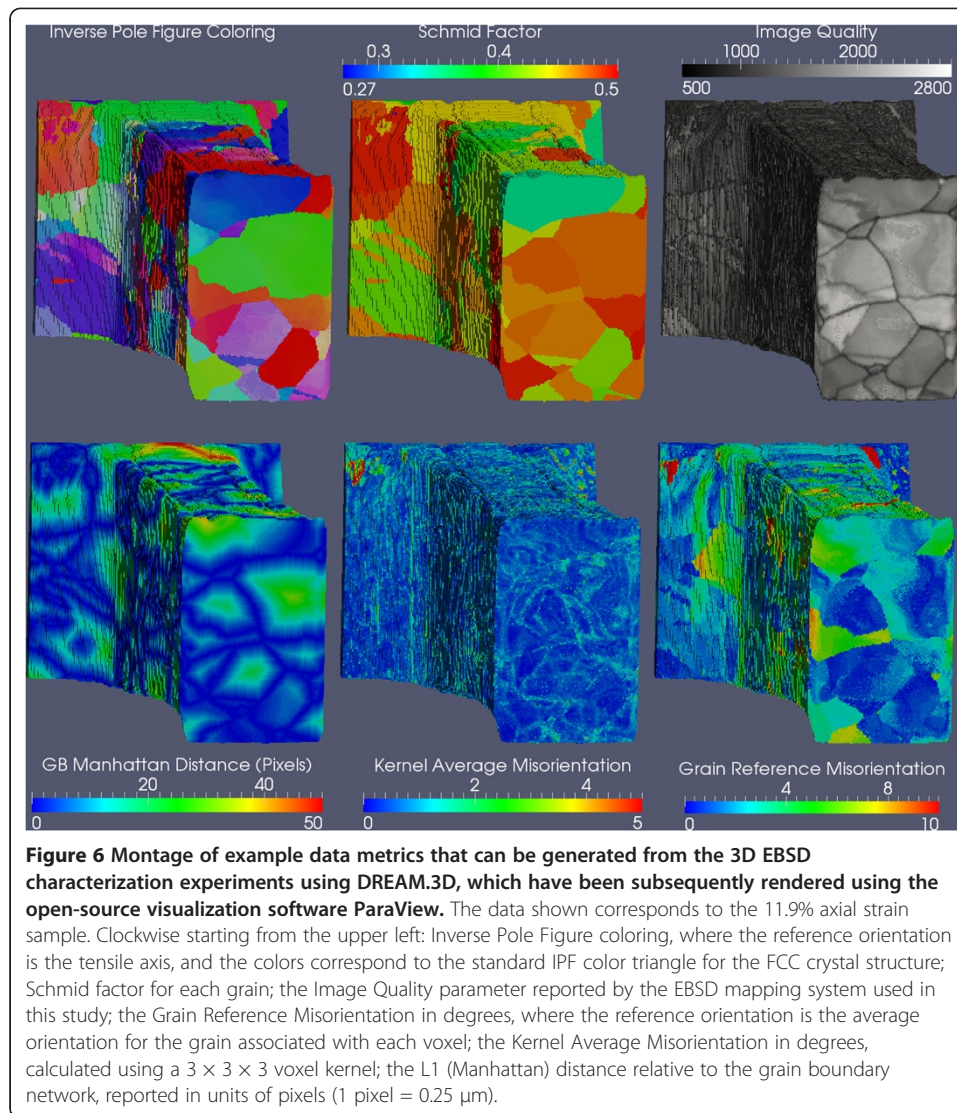
translations were removed by calculating the center-of-mass of the sample in each section, and aligning these coordinates to a common reference line. For these experiments, the common reference line corresponds to the tensile axis, which was normal to the serial sectioning plane. Following this procedure, the 3D reconstruction of the sample volume contained some visible alignment artifacts due to erroneous data points affecting the center-of-mass calculation, most noticeably at the gage-to-grip transition between the sample and the substrate. In this region of the sample, the nearby surfaces of the substrate that are in the view field of the EBSD scan (but not part of the cross-section surface) generate indexed EBSD data. These erroneous points were removed using a combination of automatic and manual filters to identify these voxels as empty space. Section-to-section translations were re-calculated using the center-of-mass alignment procedure, producing 3D volumes that contained minimal registration artifacts, as shown in Figure 5. Note that prior to performing the serial sectioning experiment on the sample shown in Figure 5A, two longitudinal and three slanted lines were FIB-milled into the top surface of the microsample before deposition of the protective platinum cap. These linear features are clearly visible in the 3D reconstruction, highlighting the accuracy of the data registration procedure.

After completing the registration process, the internal grain structure was segmented in DREAM.3D using a disorientation criteria, where sample voxels were iteratively grouped into fields (grains) when the disorientation between neighboring voxels was less than a user-defined angular threshold, here 5 degrees. This segmentation resulted in the definition of the internal grain structure, however, additional clean-up steps were required to re-assign internal data points that were deemed as erroneous, often the result of indexing errors or from identification as bad data via the original multi-threshold criteria. These features were removed from the data volume and the corresponding voxels were re-assigned using minimum size filters in DREAM.3D, where these filters were set to an ad-hoc threshold size of 16 voxels, corresponding to a volume of  $0.25 \mu\text{m}^3$ . Lastly, a combination of a 1 voxel erosion/dilation morphological filter and a surface smoothing filter were used to eliminate one-voxel wide lines and trenches on the surface of the sample. This latter filter operates by iteratively examining the coordination number of all surface voxels, and altering them by either removing voxels that have a high coordination number with the empty space, or by performing the reverse by filling empty space voxels that have a high coordination number with the sample. The 3D reconstruction of the sample deformed to 2.5% axial strain, along with engineering stress – engineering strain data and SEM images from the micro-tensile test used to calculate surface strain maps, have been made publically available [41].

After data clean-up, additional calculations were performed in DREAM.3D on the data volumes, and these metrics can be assigned to each of the fields (grains) and/or voxels that comprise the tensile volume. For example, the inverse pole figure (IPF) coloring relative to the tensile axis, is shown in Figure 5 (also included in the online version of this manuscript as Additional files 4 and 5). Figure 6 shows multiple 3D reconstructions of one of the tensile samples (which achieved a total strain of 11.9%), demonstrating additional metrics that can be calculated and displayed, in concert with other quantities that are measured as part of the EBSD acquisition process such as Image Quality [40]. Specifically, the following metrics are shown in Figure 6: Schmid factor for each grain (assuming a state of uniaxial tension), the average disorientation



of each voxel relative to its local neighborhood (Kernel Average Misorientation, 1<sup>st</sup> nearest neighbor shell), the voxel disorientation relative to a reference grain orientation, here the average orientation of each grain (Grain Reference Misorientation), the Manhattan Distance for each voxel relative to the grain boundary network, IPF coloring, and Image Quality. This data is also displayed online as a movie in Additional file 6. These examples clearly demonstrate the fidelity and complexity with which the internal crystallographic structure of the test volume can be characterized after testing, and, coupled to the surface strain maps and test volumes with controlled boundary conditions, provide a rich palette of data to link the evolution of surface deformations to both the far-field stress state and the underlying microstructure.



## Conclusion

In the present study, we demonstrated a new methodology for generating high-fidelity mechanical test data sets combined with explicit 3D microstructure representation of the entire test specimen, with the intent to couple this data to simulations for model validation and development. This was accomplished utilizing a micro-scale mechanical test specimen, so that the test volumes were amenable to examination via an established 3D microstructure characterization technique, 3D-EBSD serial sectioning with a FIB-SEM. Future studies may collect similar data on larger (mm-scale) samples by utilizing emerging destructive [42] and nondestructive [43] microstructure characterization techniques.

Surface strain distributions and internal lattice rotations were measured, and will serve as metrics from which to compare to simulations in future validation studies. One caveat to using this data for validation studies is that only the microstructure from the deformed specimen can be measured, as 3D-EBSD serial sectioning is a destructive process. Hence, some assumptions will have to be made in terms of assigning initial

orientations to the individual grains (removing internal lattice rotations due to deformation), and also the initial grain morphology (since the measured microstructure will be distorted due to the deformation). The usefulness of this technique for validation studies is therefore likely best at lower total strain values.

### Availability of supporting data

The 3D reconstruction of the sample deformed to 2.5% axial strain, along with engineering stress – engineering strain data and SEM images from the micro-tensile test used to calculate surface strain maps, have been made publically available [41].

### Additional files

**Additional file 1: Video showing evolution of surface strains during micro-tension test of the sample deformed to 1.1% axial plastic strain.** Top left is the axial (XX) strain component; middle left is the transverse (YY) strain component; bottom left is the in-plane shear (XY) strain component; top right shows the engineering stress versus axial engineering strain curve; bottom right shows the deforming sample.

**Additional file 2: Video showing evolution of surface strains during micro-tension test of the sample deformed to 2.5% axial plastic strain.** Top left is the axial (XX) strain component; middle left is the transverse (YY) strain component; bottom left is the in-plane shear (XY) strain component; top right shows the engineering stress versus axial engineering strain curve; bottom right shows the deforming sample.

**Additional file 3: Video showing evolution of surface strains during micro-tension test of the sample deformed to 11.9% axial plastic strain.** Top left is the axial (XX) strain component; middle left is the transverse (YY) strain component; bottom left is the in-plane shear (XY) strain component; top right shows the engineering stress versus axial engineering strain curve; bottom right shows the deforming sample.

**Additional file 4: 3D reconstruction of the sample deformed to 11.9% axial plastic strain.** Voxel colors represent the local inverse pole figure orientation relative to the tensile axis, and the units listed on the 3D scale bar are in micrometers.

**Additional file 5: 3D reconstruction of the sample deformed to 2.5% axial plastic strain.** Voxel colors represent the local inverse pole figure orientation relative to the tensile axis, and the units listed on the 3D scale bar are in micrometers.

**Additional file 6: Montage of example data metrics that can be generated from the 3D EBSD characterization experiments using DREAM.3D, which have been subsequently rendered using the open-source visualization software ParaView.** The data shown corresponds to the 11.9% axial strain sample. Clockwise starting from the upper left: Inverse Pole Figure coloring, where the reference orientation is the tensile axis, and the colors correspond to the standard IPF color triangle for the FCC crystal structure; Schmid factor for each grain; the Image Quality parameter reported by the EBSD mapping system used in this study; the Grain Reference Misorientation in degrees, where the reference orientation is the average orientation for the grain associated with each voxel; the Kernel Average Misorientation in degrees, calculated using a  $3 \times 3 \times 3$  voxel kernel; the L1 (Manhattan) distance relative to the grain boundary network, reported in units of pixels (1 pixel = 0.25  $\mu\text{m}$ ).

### Competing interests

The authors declare that they have no competing interests.

### Authors' contributions

The micro-tensile samples were fabricated by PS and MU. The mechanical test was conducted by PS, MG, and MU. The surface strain analysis was conducted by PS and JS. The 3D EBSD serial section data was collected by PS, MG, and MU. The 3D EBSD reconstructions were conducted by MG and MU. All authors have read and approved the final manuscript.

### Acknowledgements

The authors would like to thank Dr. R. Wheeler (UES Inc., MicroTesting Solutions LLC) who developed the micro-testing device used in these experiments, and Adam Shiveley (UES, Inc.) for help setting up communication between various instrument computers. The authors would also like to acknowledge useful discussions with Drs. D.M. Dimiduk (Air Force Research Laboratory), T.J. Turner (Air Force Research Laboratory), and Y.S. Choi (UES Inc.). The authors acknowledge support from the Air Force Office of Scientific Research (AFOSR, program managers Dr. Joan Fuller and Dr. Ali Sayir) and the Materials & Manufacturing Directorate of the Air Force Research Laboratory.

Received: 25 September 2013 Accepted: 1 November 2013

Published: 18 November 2013

## References

1. Roters F, Eisenlohr P, Hantcherli L, Tjahjanto DD, Bieler TR, Raabe D (2010) Overview of constitutive laws, kinematics, homogenization and multiscale methods in crystal plasticity finite-element modeling: Theory, experiments, applications. *Acta Mater* 58:1152–1211
2. Lim H, Lee MG, Kim JH, Adams BL, Wagoner RH (2011) Simulation of polycrystal deformation with grain and grain boundary effects. *Int J Plast* 27:1328–1354
3. Uchic MD, Dimiduk DM, Florando JN, Nix WD (2004) Sample dimensions influence strength and crystal plasticity. *Science* 305:986–989
4. McDowell DL (2008) Viscoplasticity of heterogeneous metallic materials. *Mater Sci Eng R* 62:67–123
5. Becker R, Panchanadeeswaran (1995) Effects of grain interactions on deformation and local texture in polycrystals. *Acta Metall Mater* 43:2701–2719
6. Bhattacharyya A, El-Danaf E, Kalidindi SR, Doherty RD (2001) Evolution of grain-scale microstructure during large strain simple compression of polycrystalline aluminum with quasi-columnar grains: OIM measurements and numerical simulations. *Int J Plast* 17:861–883
7. Cheong KS, Busso EP (2006) Effects of lattice misorientations on strain heterogeneities in FCC polycrystals. *J Mech Phys Solids* 54:671–689
8. Heripre E, Dextet M, Crepin J, Gelebart L, Roos A, Bornert M, Caldemaison D (2007) Coupling between experimental measurements and polycrystal finite element calculations for micromechanical study of metallic materials. *Int J Plast* 23:1512–1539
9. Kalidindi SR, Bhattacharyya A, Doherty RD (2004) Detailed analyses of grain-scale plastic deformation in columnar polycrystalline aluminium using orientation image mapping and crystal plasticity models. *Proc Roy Soc Lond A* 460:1935–1956
10. Rehr C, Volkert B, Kleber S, Antretter T, Pippan R (2012) Crystal orientation changes: A comparison between a crystal plasticity finite element study and experimental results. *Acta Mater* 60:2379–2386
11. Turner TJ, Semiatin SL (2011) Modeling large-strain deformation behavior and neighborhood effects during hot working of a coarse-grain nickel-base superalloy. *Model Simul Mater Sci Eng* 19:065010
12. Zhao Z, Ramesh M, Raabe D, Cuitino AM, Radovitzky R (2008) Investigation of three-dimensional aspects of grain-scale plastic surface deformation of an aluminum oligocrystal. *Int J Plast* 24:2278–2297
13. St-Pierre L, Heripre E, Dextet M, Crepin J, Bertolino G, Bilger N (2008) 3D simulations of microstructure and comparison with experimental microstructure coming from O.I.M. analysis. *Int J Plast* 24:1516–1532
14. Musienko A, Tatschl A, Schmidegg K, Kolednik O, Pippan R, Cailletaud G (2007) Three-dimensional finite element simulation of a polycrystalline copper specimen. *Acta Mater* 55:4121–4136
15. Gianola DS, Eberl C (2009) Micro- and nanoscale tensile testing of materials. *JOM* 61:24–35
16. Kiener D, Grosinger W, Dehm G, Pippan R (2008) A further step towards an understanding of size-dependent crystal plasticity: In situ tension experiments of miniaturized single-crystal copper samples. *Acta Mater* 56:580–592
17. Kim JY, Greer JR (2009) Tensile and compressive behavior of gold and molybdenum single crystals at the nano-scale. *Acta Mater* 57:5245–5253
18. Wheeler R, Shade PA, Uchic MD (2012) Insights gained through image analysis during in-situ micromechanical experiments. *JOM* 64:58–65
19. Peters WH, Ranson WF (1982) Digital imaging techniques in experimental stress analysis. *Opt Eng* 21:427–432
20. Sutton MA, Wolters WJ, Peters WH, Ranson WF, McNeill SR (1983) Determination of displacements using an improved digital correlation method. *Image Vision Comput* 1:133–139
21. Sutton MA, Li N, Joy DC, Reynolds AP, Li X (2007) Scanning electron microscopy for quantitative small and large deformation measurements Part I: SEM imaging at magnifications from 200 to 10,000. *Exp Mech* 47:775–787
22. Wissuchek DJ, Mackin TJ, DeGraef M, Lucas GE, Evans AG (1996) A simple method for measuring surface strains around cracks. *Exp Mech* 36:173–179
23. Biery N, De Graef M, Pollock TM (2003) A method for measuring microstructural-scale strains using a scanning electron microscope: Applications to  $\gamma$ -titanium aluminides. *Metall Mater Trans A* 34:2301–2313
24. Uchic MD, Groeber M, Wheeler R, Scheltens F, Dimiduk DM (2004) Augmenting the 3D characterization capability of the dual beam FIB-SEM. *Microsc Microanal* 10(Suppl 2):1136–1137
25. Groeber MA, Haley BK, Uchic MD, Dimiduk DM, Ghosh S (2006) 3D reconstruction and characterization of polycrystalline microstructures using a FIB-SEM system. *Mater Charact* 57:259–273
26. Uchic MD, Groeber MA, Dimiduk DM, Simmons JP (2006) 3D microstructural characterization of nickel superalloys via serial-sectioning using a dual beam FIB-SEM. *Scripta Mater* 55:23–28
27. Zafarani N, Raabe D, Singh RN, Roters F, Zaefferer S (2006) Three-dimensional investigation of the texture and microstructure below a nanoindent in a Cu single crystal using 3D EBSD and crystal plasticity finite element simulations. *Acta Mater* 54:1863–1876
28. Turner TJ, Shade PA, Groeber MA, Schuren JC (2013) The influence of microstructure on surface strain distributions in a nickel micro-tension specimen. *Model Simul Mater Sci Eng* 21:015002
29. Shade PA, Kim SL, Wheeler R, Uchic MD (2012) Stencil mask methodology for the parallelized production of microscale mechanical test samples. *Rev Sci Instrum* 83:053903
30. Uchic MD, Dimiduk DM, Wheeler R, Shade PA, Fraser HL (2006) Application of micro-sample testing to study fundamental aspects of plastic flow. *Scripta Mater* 54:759–764
31. Shade PA, Wheeler R, Choi YS, Uchic MD, Dimiduk DM, Fraser HL (2009) A combined experimental and simulation study to examine lateral constraint effects on microcompression of single-slip oriented single crystals. *Acta Mater* 57:4580–4587
32. Jones RV (1951) Parallel and rectilinear spring movements. *J Sci Instrum* 28:38–41
33. Jones RV, Young IR (1956) Some parasitic deflexions in parallel spring movements. *J Sci Instrum* 33:11–15
34. Wu A, De Graef M, Pollock TM (2006) Grain-scale strain mapping for analysis of slip activity in polycrystalline B2 RuAl. *Phil Mag* 86:3995–4008
35. Orloff J, Utlaut M, Swanson L (2003) High resolution focused ion beams: FIB and its applications. Kluwer Academic/Plenum, New York

36. Wilkinson AJ, Meaden G, Dingley DJ (2006) High-resolution elastic strain measurement from electron backscatter diffraction patterns: New levels of sensitivity. *Ultramicroscopy* 106:307–313
37. Bhandari Y, Sarkar S, Groeber M, Uchic MD, Dimiduk DM, Ghosh S (2007) 3D polycrystalline microstructure reconstruction from FIB generated serial sections for FE analysis. *Comput Mater Sci* 41:222–235
38. Ghosh S, Bhandari Y, Groeber M (2008) CAD-based reconstruction of 3D polycrystalline alloy microstructures from FIB generated serial sections. *CAD* 40:293–310
39. DREAM.3D. <http://dream3d.bluequartz.net/>
40. Schwartz AJ, Kumar M, Adams BL (2000) *Electron backscatter diffraction in materials science*. Kluwer Academic/Plenum, New York
41. Shade PA, Groeber MA, Schuren JC, Uchic MD (2013) 3D microstructure reconstruction of polycrystalline nickel micro-tension test. <http://hdl.handle.net/11115/152>
42. Uchic M, Groeber M, Shah M, Callahan P, Shiveley A, Scott M, Chapman M, Spowart J (2012) An automated multi-modal serial sectioning system for characterization of grain-scale microstructures in engineering materials. In: De Graef M, Poulsen HF, Lewis A, Simmons J, Spanos G (ed) 1st International Conference on 3D Materials Science, pp 195–202
43. Suter RM, Hennessy D, Xiao C, Lienert U (2006) Forward modeling method for microstructure reconstruction using x-ray diffraction microscopy: single crystal verification. *Rev Sci Instrum* 77:123905

doi:10.1186/2193-9772-2-5

**Cite this article as:** Shade et al.: Experimental measurement of surface strains and local lattice rotations combined with 3D microstructure reconstruction from deformed polycrystalline ensembles at the micro-scale. *Integrating Materials and Manufacturing Innovation* 2013 **2**:5.

Submit your manuscript to a SpringerOpen<sup>®</sup> journal and benefit from:

- Convenient online submission
- Rigorous peer review
- Immediate publication on acceptance
- Open access: articles freely available online
- High visibility within the field
- Retaining the copyright to your article

---

Submit your next manuscript at ► [springeropen.com](http://springeropen.com)

---